Fuzzy Fractional Order Force Control of 6PUS-UPU Redundantly Actuated Parallel Robot Based on Inner Model Position Control Structure

Shuhuan Wen, Baowei Zhang, Pengcheng Hao, Hak-keung Lam, Hongbin Wang

***Abstract*—The 6PUS-UPU parallel robot is a kind of multi-input multi-output, coupled and highly nonlinear system. Conventional control methods are no longer effective for this complex 6PUS-UPU parallel robot. In this paper, the Inner Model Control (IMC) method in the position control loop and the Fractional Order Fuzzy Proportional Integral Derivative (FOPID) control method in the force loop are investigated. To study the validness of the IMC method and the FOPID control method, their performance is compared with other published control methods under disturbance and noise, such as three-loop control method, PI control method and Fuzzy Proportional-Integral-Derivative control method. The simulation results clearly demonstrate that the robustness of IMC method and the FOPID control method outperform other methods.**

***Index Terms*—Parallel robot, Fuzzy control, Fractional order, Inner model control**

I. Introduction

PARALLEL Manipulator (PM) [1] is a product created by the combination of parallel mechanism principle with modern robot technique. Compared to the traditional machine, it has many advantages, such as high speed, high precision, high stiffness etc.. A lot of problems arise because of the multiple-input-multiple-output (MIMO) characteristic of the parallel manipulator and environment uncertainty, for instance, strong coupling between each branch of the parallel manipulator, smaller workspace, singularity etc.. Finally it may lead to uncertainly huge internal force which may damage the machine.

This work is partly supported by the National Natural Science Foundation of China (Project No.51275439 and No.61473248), and the Major State Basic Research Development Program of China 973 program (Project No. 2013CB733000), the Natural Science Foundation of Hebei Province of China (Project No.F2014203095), China Postdoctoral Science Foundation (Project No. 2014M560196), Scholars Studying Abroad Science and Technology Activities of Hebei Province of China (Project No. C201400355) and the Young Teacher of Yanshan University under the project No.13LGA007.

Shuhuan Wen, Baowei Zhang, Pengcheng Hao and Hongbin Wang are with the department of Key Lab of Industrial Computer Control Engineering of Hebei Province, Yanshan University, Qinhuangdao, 066004, China, e-mail: swen@ysu.edu.cn, 458110801@qq.com, 787701548@qq.com, hb_wang@ysu.edu.cn

H.K. Lam is with the department of Informatics, Kings College London, Strand, London, WC2R 2LS, United Kingdom, e-mail: hak-keung.lam@kcl.ac.uk.

Because the input numbers of redundant actuation parallel robot is bigger than its degrees of freedom, the errors resulting from processing, assembling or moving will make the machine deformation and damage the machine if all inputs are used in the position control mode. If all actuators are force control mode, there must be an accurate dynamic model parameters, such as friction coefficient which is difficult to obtain in practice, especially for complex space multi-freedom robots. The dynamics expression of 6-PUS/UPU redundant actuation parallel robot is very complex and needs a lot of calculations. It is not easy to implement real-time control. So it is fit for complex multi-DOF (Degrees of Freedom) redundant actuation parallel robot to use hybrid force/position control strategy. The redundant actuator uses force control mode, while other drive actuators use position control mode. Position control can ensure the accuracy of the position and orientation of the moving platform, while force control can adjust the distribution of actuating torque. Then the position control and force control are decoupled.

However, the existing literature for the control strategy of the redundant actuation parallel robot is seldom studied. To some extent, it limits its operation, the improvement of high precision, high-quality, real-time in the production process. Existing literatures for the research work of the parallel robot control system are mainly in Kinematic control method of parallel robot [2], Dynamic control method based on Parallel Robot [3] Nonlinear position control of parallel robot control system [4, 5], Force/position control structure performance analysis of parallel robot [6].

PMSM (Permanent Magnet Synchronous Motor) is widely used in industries because of its compact structure, high power density, high torque/inertia ratio and absence of rotor losses. Vector control method is a kind of commonly used control theory for PMSM servo system. As a kind of typical real time control system, the PMSM servo system includes current loop, speed loop and position loop. In general, almost all these three loops adopt regular PID controller. The reason is that the structure of this controller is simple and it is easily realized. However, as a kind of one degree controller, its performance is very sensitive to parameter variations and external disturbances [7].

Internal model control (IMC) method is proposed by Garcia and Morari formally in 1982 [8]. IMC method is used widely in many industry environments. In [9], the authors studied single-phase voltage source uninterrupted power supply (UPS) inverter and proposed a kind of novel control scheme which possessed two feedback closed loops. The external loop combined the IMC and PID controller to ensure stable performance and suppressed waveform distortion. The work in [10] applied the IMC method to high-precision hydraulic servo system, the inner loop adopted P controller and the IMC method were used in the external loop. The experiment results indicated that the double closed-loop IMC-PID control method did well in tracking performance, anti-interference and robustness performance. In [11], the authors designed a kind of nonlinear IMC controller based on Cartesian signal and applied the nonlinear IMC method to linearize high frequency power amplifiers (PAs). And the results showed that it could reduce the influence of nonlinearity and time-delay. The authors of [12] proposed a kind of IMC method with conditional integrator for the robust output regulation of single-switch quadratic buck converters and analyzed the closed-loop stability of converters. The experiments results indicated that the proposed control scheme was effective for the large load disturbance and supply variations.

Conventional PID control is the most widely used and the most mature technology in control system, and the quality of PID controller directly affect the process of industrial control effect. The combination of fractional order theory and PID controller tuning theory is a new research direction. In recent years, the fractional order has received more and more attention of the researchers. The significant research in the field of fractional order PID (FOPID) controllers has been developed by several authors. To further improve the dynamic and robustness performance, in [13], a fractional-order PD^{α} controller is proposed, the exactly stable regions of delays are explored for both integral-order and fractional-order controllers. The authors of [14] proposed a fractional-order $PI^{\lambda}D^{\mu}$-controller, including fractional-order integrator and fractional-order differentiator, it included arbitrary order differential and integral. In [15], the authors proposed a kind of fractional order fuzzy-PID controller for the piezoelectric actuators (PEA) to deal with the hysteresis nonlinearity problem. The simulations results validated the proposed approach and showed that the proposed controller presents better performances compared to well tuned classical PID and fuzzy PID controllers. The authors of [16] proposed a kind of FOFPID controller and Genetic Algorithm was used to tune the parameters. In this paper, the effectiveness and robustness of the proposed controller is discussed, by applying two fractional order systems. The results showed in all cases discussed that the results of fractional fuzzy controller is better than the results of FOPID controller. The authors of [17, 18] applied the FOFPID controller to the delayed nonlinear systems and open loop unstable process with time delay. The simulation results for FOFPID, FPID, FOPID and PID controllers for the different performance indices were discussed and also studied performance comparison of set-point tracking, load disturbance and small control signal.

This work has the following novelties. Compared to other works in the literature, as in [9–12], we use an IMC control method with two degrees of freedom to enhance the position control accuracy and interference immunity in the position tracking control. The works in [9–12] only adjust one parameter λ which decides the robustness and dynamic performance of the system. Although it is convenient to adjust the parameter, the parameter adjustment needs to compromise between the dynamic performance and robustness. So in this paper we propose a kind of two degrees of freedom IMC control method, which uses two parameters to adjust the dynamic performance and robustness of the system. However, the two parameters are interplay. When the parameter deciding the anti-interference performance is adjusted, the dynamic performance of the system will be also influenced. So it is necessary to determine a parameter based on the anti-interference performance, and then determine another parameter according to the dynamic performance. So IMC control method is used to separate the two parameters. One parameter is connected with the dynamic performance, the other parameter is connected with the robustness. Then we could adjust the dynamic performance and robustness independently. We also compare the IMC performance with conventional three-loop control. The IMC control method has stronger robustness and less error than the three-loop control method. After that, we integrate the Fuzzy-PID control method with fractional order differential and integral operators, then propose a kind of Fractional Order Fuzzy-PID control method. Finally, the simulation show the performance of IMC and Fractional Order Fuzzy-PID controllers outperformed in terms of the driving forces and pose errors.

The paper is organized as follows. We first present the model of 6PUS-UPU redundant auction parallel robot. Afterward, KANE method and optimization of the driving forces are explained in Section II. Then, Section III, deals with the IMC and FOFPID control of the parallel manipulator. Simulation results are discussed in Section IV and finally some comments conclude the work in Section V.

II. Dynamic modeling

In this section, we will analyze the model of 6PUS-UPU redundant actuation parallel robot based on KANE method and optimization of the driving force.

Fig. 1 shows the model and the coordinate system of 6PUS-UPU redundant actuation parallel robot. It consists of a movable platform, a fixed platform, six actuators connecting

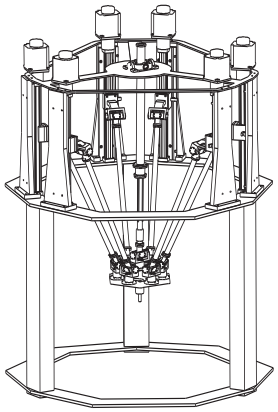

Fig. 1: The model of 6PUS-UPU redundant actuation parallel robot.

with the movable platform and the fixed platform, and a constraint branch. The six actuators connect with the movable platform and the fixed platform by the prismatic pair (P), universal joint (U), and spherical hinge (S). The constraint branch connects with the two platforms by the universal joint (U).

The velocity, acceleration, partial velocity, constrain analysis are shown in Appendix.

A. KANE Equation

Generalized velocity consists of six components. We suppose each component's generalized force as $\boldsymbol{F}_j$, and the generalized initial force as $\boldsymbol{F}_j^*$, the driving force of the six branches as $\boldsymbol{F}_{qi}$, the constraints of the middle branch as $\boldsymbol{M}_c$, and external force and torque as $\boldsymbol{F}$ and $\boldsymbol{M}$, respectively. Then we can get the following equations

$$\begin{aligned}\boldsymbol{F}_j^r = m_d\boldsymbol{g}\boldsymbol{v}_{d,j}^* + \boldsymbol{F}\boldsymbol{v}_{d,j}^* + \boldsymbol{M}\boldsymbol{\omega}_{d,j}^* + \sum_{i=1}^{6} m_{Hi}\boldsymbol{g}\boldsymbol{v}_{Hi,j}^* + \\ \sum_{i=1}^{6}\boldsymbol{F}_{qi}\boldsymbol{J}_{Hi,j} + \boldsymbol{M}_c\boldsymbol{v}_{d,j}^* + \sum_{i=1}^{6} m_{Li}\boldsymbol{g}\boldsymbol{v}_{Li,j}^* + \\ m_{zu}\boldsymbol{g}\boldsymbol{v}_{zu,j}^* + m_{zl}\boldsymbol{g}\boldsymbol{v}_{zd,j}^*,\end{aligned} \tag{1}$$

$$\begin{aligned}\boldsymbol{F}_j^{*r} = &- m_d\boldsymbol{a}_d\boldsymbol{v}_{d,j}^* - \sum_{i=1}^{6}\boldsymbol{m}_{Hi}\boldsymbol{a}_{Hi}\boldsymbol{v}_{Hi,j}^* - \sum_{i=1}^{6}\boldsymbol{m}_{Li}\boldsymbol{a}_{Li}\boldsymbol{v}_{Li,j}^* - \\ &m_{zu}\boldsymbol{a}_{zu}\boldsymbol{v}_{zu,j}^* - m_{zl}\boldsymbol{a}_{zl}\boldsymbol{v}_{zl,j}^* - (\boldsymbol{I}_d\boldsymbol{\varepsilon}_d + \boldsymbol{\omega}_d\times\boldsymbol{I}_d\boldsymbol{\omega}_d)\boldsymbol{\omega}_{d,j}^* - \\ &\sum_{i=1}^{6}\big(\boldsymbol{I}_{Li}\boldsymbol{\varepsilon}_{Li} + \boldsymbol{\omega}_{Li}\times\boldsymbol{I}_{Li}\boldsymbol{\omega}_{Li}\big)\boldsymbol{\omega}_{Li,j}^* - (\boldsymbol{I}_{zu}\boldsymbol{\varepsilon}_{Lz} + \\ &\boldsymbol{\omega}_{Lz}\times\boldsymbol{I}_{zu}\boldsymbol{\omega}_{Lz})\boldsymbol{\omega}_{Lz}^* - (\boldsymbol{I}_{zl}\boldsymbol{\varepsilon}_{Lz} + \boldsymbol{\omega}_{Lz}\times\boldsymbol{I}_{zl}\boldsymbol{\omega}_{Lz})\boldsymbol{w}\end{aligned} \tag{2}$$

where m_d is the mass of the movable platform, m_{Hi} is the mass of each slider, m_{Li} is the mass of the link, m_{zu} and m_{zl} are the mass of the upper and lower link of the middle constraint branch, respectively; $\boldsymbol{I}_d$ and $\boldsymbol{I}_{Li}$ are movable platform initial matrix and link initial matrix, respectively, $\boldsymbol{I}_{zu}$ and $\boldsymbol{I}_{zl}$ are the initial matrix of the upper and lower link, respectively.

So, the KANE equation can be expressed as

$$\begin{aligned}\boldsymbol{F}^r + \boldsymbol{F}^{*r} = \boldsymbol{G}\big[\ \boldsymbol{F}_{q1}\quad \boldsymbol{F}_{q2}\quad \boldsymbol{F}_{q3}\quad \boldsymbol{F}_{q4}\quad \boldsymbol{F}_{q5}\quad \boldsymbol{F}_{q6}\quad \boldsymbol{M}_c\ \big]^T \\ -\boldsymbol{F}'^T = 0\end{aligned} \tag{3}$$

where $\boldsymbol{G}$ is the Jacobian matrix between the driving forces and platform, $\boldsymbol{\tau}$ is the driving force vector, $\boldsymbol{F}'^T$ is the rest part of the KANE equation.

The 6PUS-UPU parallel robot possesses 5 degrees of freedom, but meanwhile it is provided with 6 inputs, which means there exists infinite input solutions in each motion. This is one of the reasons that the machine is so complicated. In general, there are two methods to optimize the driving forces [19]. One is force optimization, the other is energy optimization. Though the energy optimization could enhance the system efficiency, it will also result in high fluctuation for driving forces. The main problem existing in 6PUS-UPU parallel robot is how to balance the inner forces and then promote the precision of the movable platform. So in this paper we select the force optimization method to optimize the driving forces.

The driving force optimization problem can be described as following.

$$\begin{cases}\min\ \boldsymbol{Z} = \boldsymbol{\tau}^T\boldsymbol{W}\boldsymbol{\tau} \\ s.t.\ \boldsymbol{G}\boldsymbol{\tau} = \boldsymbol{F}'^T\end{cases} \tag{4}$$

where $\boldsymbol{W}$ is a diagonal weighted matrix. We introduce the Lagrangian multiplier λ to construct a new equation.

$$\boldsymbol{Z}' = \boldsymbol{\tau}^T\boldsymbol{W}\boldsymbol{\tau} + \boldsymbol{\lambda}^T\left(\boldsymbol{F}'^T - \boldsymbol{G}\boldsymbol{\tau}\right) \tag{5}$$

(5) must satisfy the following conditions.

$$\begin{cases}\frac{\partial\boldsymbol{Z}'}{\partial\boldsymbol{\tau}} = 2\boldsymbol{\tau}^T\boldsymbol{W} - \boldsymbol{\lambda}^T\boldsymbol{G} = 0 \\ \frac{\partial\boldsymbol{Z}'}{\partial\boldsymbol{\lambda}} = \boldsymbol{F}'^T - \boldsymbol{G}\boldsymbol{\tau} = 0\end{cases} \tag{6}$$

Then we can derive (7) from (5) to (6).

$$\boldsymbol{\tau} = \left(\boldsymbol{W}^{-1}\right)\boldsymbol{G}^T\left(\boldsymbol{G}\left(\boldsymbol{W}^{-1}\right)\boldsymbol{G}^T\right)^{-1}\boldsymbol{F}'^T \tag{7}$$

Then we can get (8).

$$\begin{aligned}\boldsymbol{\tau} &= \boldsymbol{G}^T\left(\boldsymbol{G}\boldsymbol{G}^T\right)^{-1}\boldsymbol{F}'^T \\ &= \boldsymbol{G}^+\boldsymbol{F}'^T\end{aligned} \tag{8}$$

where $\boldsymbol{G}$ is a non-invertible matrix, $\boldsymbol{G}^+$ is the pseudo-inverse matrix of $\boldsymbol{G}$.

III. Control Design

Task-space control [20] and joint-space control [21] are two common schemes applied in MIMO system. Considering the computational burden and experimental applications, the joint-space control is preferable [22]. However, it is difficult to apply this control scheme to the 6PUS-UPU redundant actuation parallel robot in real situation. The 6PUS-UPU redundant actuation parallel robot has a redundant branch that it will aggravate coupling situation and increase internal force. Under the heavy load and high-speed situation, it is easy to damage the device because of the branch error and instant opposite

reaction force. Force/position hybrid control is a common control scheme for the 6PUS-UPU. Considering the structure of 6PUS-UPU redundant actuation parallel robot, we can use the redundant branch to supply extra compensation dosage to compensate the influence caused by the uncertainty of the dynamics model and friction. The control structure diagram is shown as Fig. 2.

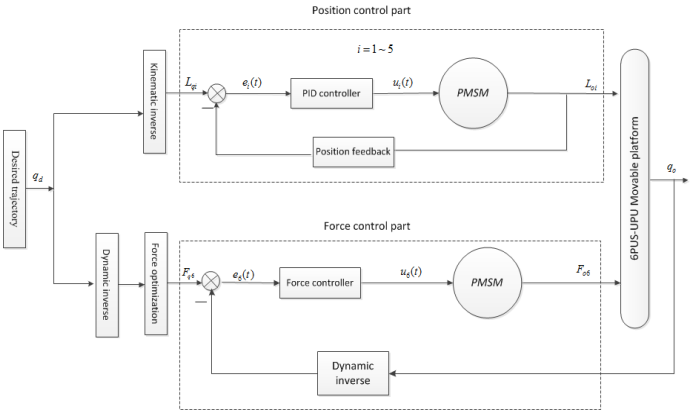

Fig. 2: The control structure diagram of 6PUS-UPU redundant actuation parallel robot.

As the Fig. 2 shows, the first five branches adopt position control scheme, and the sixth branch adopts force control scheme. The force feedback in Fig. 2 shows is calculated based on the dynamic model obtained in the Section II. This structure introduces the real time motion state of the movable platform and realizes local closed-loop.

A. Position control design

Vector Control Method promotes the performance of AC servo system. It makes the AC servo system possess excellent performance as good as the DC motor. So in the field of industry robot, AC servo system is used more commonly. Because of simple structure and easily realized, three-loop control method is used in most AC servo system. The diagram of three-loop control method is shown in Fig. 3.

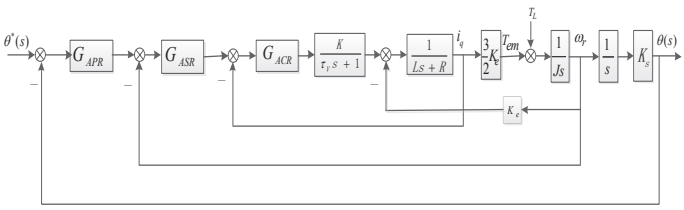

Fig. 3: The Three-loop control method diagram.

where G_{APR}, G_{ASR} and G_{ACR} represent the position loop, speed loop and current loop controllers, respectively. The G_{ASR} and G_{ACR} are the conventional PI controller, and the G_{APR} is the P controller. $\frac{K}{\tau_V s+1}$ (K represents the inverter magnification, τ_V represents the time constant) is the simplified transfer function of the PWM inverter [23]. $\frac{1}{Ls+R}$ (L represents the motor armature inductance, R represents the motor armature resistance) is the simplified transfer function of the PMSM motor. K_s is the proportionality coefficient of the ball screw. J is the motor rotor and the screw is equivalent to the rotational inertia of the motor shaft.

However, there exit some problems in the AC servo system, such as time-varying parameters, load disturb and uncertainty etc. These problems will influence the control precision. Regular PI and P controller could not meet the system requirements [24]. IMC is a common advanced control algorithm which possesses convenient parameter adjustment, strong robustness etc. [25]. In this paper, we design a kind of parameter self-adjusted inner model control algorithm to improve the position tracking precision and robustness.

The IMC diagram is shown in Fig. 4. Where $P(s)$ is the controlled object, $M(s)$ is the mathematical model of controlled object, namely the internal model, $Q(s)$ is the internal model controller, $R(s)$, $Y(s)$ and $D(s)$ respectively for the input, output, and the control system of interference signal.

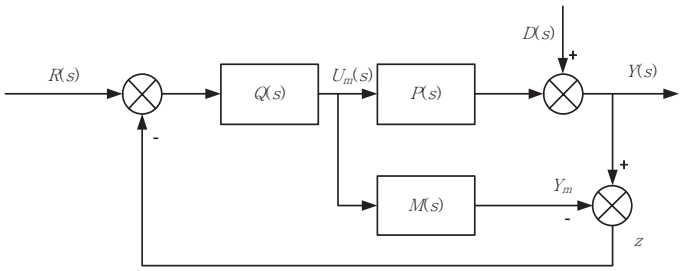

Fig. 4: The diagram of IMC control method.

Based on the Fig. 4, we can get the following two equations.

$$\frac{Y(s)}{R(s)} = \frac{Q(s)P(s)}{1+Q(s)[P(s)-M(s)]} \tag{9}$$

$$\frac{Y(s)}{D(s)} = \frac{1-Q(s)M(s)}{1+Q(s)[P(s)-M(s)]} \tag{10}$$

Then we can get the closed loop response.

$$\begin{aligned} Y(s) = &\frac{Q(s)P(s)}{1+Q(s)[P(s)-M(s)]}R(s)+ \\ &\frac{1-Q(s)M(s)}{1+Q(s)[P(s)-M(s)]}D(s) \end{aligned} \tag{11}$$

For the IMC system, if $Q(s) = M^{-1}(s)$, we will get very good tracking performance and anti-interference even without adjusting the parameters of controller. But in fact, the ideal controller is difficult to be obtained, the reasons are the followings.

1) The controlled object (or process) possesses delay part, so the $Q(s) = M^{-1}(s)$ has the pure advanced argument, which is difficult to be realized.

2) If the controlled object (or progress) has zeros in the right half-plane, the controller $Q(s)$ has poles in the right half-plane. So the controller is unstable, and this will result in instability of system.

3) If the $M(s)$ is rational, then

$$\lim_{s\to 0}|Q(s)|\to\infty. \tag{12}$$

4) The system with ideal controller is sensitive to the model error, if $P(s)\neq M(s)$ it is difficult to ensure the stability and robustness of the system.

For the above reasons, we cannot obtain the ideal controller. So we should take another way to design the controller. In general, we take the following steps to design the IMC controller.

1) Decompose $M(s)$.

$M(s)$ should be decomposed into two parts: $M_+(s)$ and $M_-(s)$. $M_+(s)$ is the pure delay and unstable part, $M_-(s)$ is the minimum phase part.

2) Design IMC control method.

To ensure the system stability, the dynamic quality and the realization of the controller, it is not feasible to only use inverse of minimum phase $M_-(s)$ of system model, we need a low pass filter. So the $Q(s)$ is rational. Tuning the parameters of the filter to ensure the performance of the system. Now we suppose that the IMC control method is the following form.

$$Q(s)=f(s){M_-}^{-1}(s) \tag{13}$$

where $f(s)$ is the low pass filter. One of the reasons we design $f(s)$ is to keep the $Q(s)$ rational, so it is designed as the following form.

$$f(s)=\frac{1}{(1+\lambda s)^r} \tag{14}$$

where r should be big enough to ensure that $Q(s)$ is rational. λ is the time parameter of the filter and it is the only parameter of the IMC control method. The system in Fig. 4 could be transformed into a conventional feedback system as shown in Fig. 5.

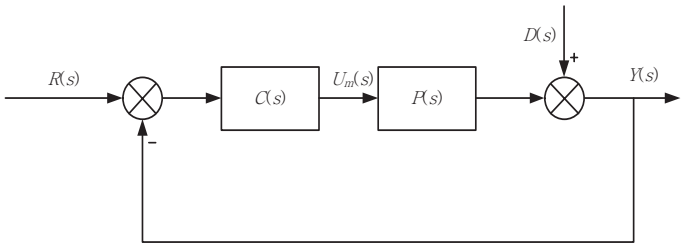

Fig. 5: The equivalent diagram of IMC control method.

$C(s)$ is the feedback controller and there exists the following relationship among $C(s)$, $M(s)$ and $Q(s)$ [26].

$$C(s)=\frac{Q(s)}{1-M(s)Q(s)} \tag{15}$$

$$Q(s)=\frac{C(s)}{1+M(s)C(s)} \tag{16}$$

Vector control system generally includes current loop, speed loop and position loop, as it is shown in the Fig. 3. Considering the system stability and simplicity [27], the speed loop and current loop could be regarded as a one-order system and it could be written as the following equation.

$$M(s)=\frac{K}{s(Ts+1)} \tag{17}$$

where T is the time constant, K is the gain of the open loop.

As it is described in [28], to obtain the PID controller form, $f(s)$ could be designed as the following equation.

$$f(s)=\frac{2\lambda s+1}{(\lambda s+1)^2} \tag{18}$$

So the the controller $C(s)$ could be written as the following equation.

$$C(s)=\frac{(2\lambda s+1)(Ts+1)}{K\lambda^2 s}=K_P+K_I\frac{1}{s}+K_D s \tag{19}$$

where $K_P=\frac{(2\lambda+T)}{K\lambda^2}$, $K_I=\frac{1}{K\lambda^2}$ and $K_D=\frac{2T}{K\lambda}$. Obviously there is only one parameter λ to be adjusted, λ decides the robustness and dynamic performance of the system. It is convenient to adjust the parameter. But the parameter adjustment needs to compromise between the dynamic performance and robustness. So in this paper we propose a kind of two degrees of freedom IMC control method [29], which satisfy both of the dynamic performance and robustness. Its diagram is shown in Fig. 6.

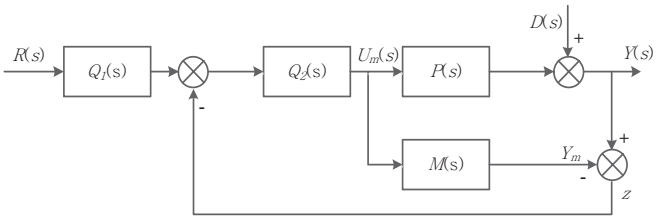

Fig. 6: The diagram of IMC control method with two degrees of freedom.

Where $Q_1(s)$ and $Q_2(s)$ constitute the two degrees of freedom IMC controller. Based on the Fig. 6, we can get the following equation.

$$\begin{aligned}Y(s)=&\frac{P(s)Q_1(s)Q_2(s)}{1+Q_2(s)[P(s)-M(s)]}R(s)+\\&\frac{1-M(s)Q_2(s)}{1+Q_2(s)[P(s)-M(s)]}D(s)\end{aligned} \tag{20}$$

Obviously, the dynamic performance is related to $Q_1(s)$ and $Q_2(s)$, and the robustness is related to $Q_2(s)$. So the dynamic performance and robustness are interplay, and we need to adjust them independently. To separate them, $Q_2(s)$ is designed as the following form.

$$Q_2(s)=M^{-1}(s)f_2(s) \tag{21}$$

where $f_2(s)$ is the low-pass filter and it is designed as the following form.

$$f_2(s) = \frac{3\lambda_2 s + 1}{(\lambda_2 s + 1)^3} \tag{22}$$

$Q_1(s)$ is designed as the following equations.

$$\begin{cases} Q_1(s) = \dfrac{f_1(s)}{f_2(s)} \\ f_1(s) = \dfrac{3\lambda_1 s + 1}{(\lambda_2 s + 1)^3} \end{cases} \tag{23}$$

In this way, the dynamic performance is only related to the $f_1(s)$, while the robustness is only related to the $f_2(s)$. We could adjust the dynamic performance and robustness independently.

B. Result analysis of position control design

To testify whether the designed controller could meet the requirement of dynamic performance and robustness, we design three simulation environments:

1) J = 6.2 $\times$ 10^{-3} $kg \cdot m^2$, T_L = 0 $N \cdot m$.

In this simulation environment, the inertial J = 6.2 $\times$ 10^{-3} $kg \cdot m^2$ and there is no load.

2) J = 6.2 $\times$ 10^{-3} $kg \cdot m^2$, T_L = 20 $N \cdot m$ (2s).

In this simulation environment, the inertial J = 6.2 $\times$ 10^{-3} $kg \cdot m^2$ and a load of 20 $N \cdot m$ is suddenly added at the time of 2 seconds.

3) J = 5.5 $\times$ 10^{-3} $kg \cdot m^2$, T_L = 20 $N \cdot m$ (2s).

In this simulation environment, the inertial variable is changed to J = 5.5 $\times$ 10^{-3} $kg \cdot m^2$, and the load of 20 $N \cdot m$ is suddenly added at the time of 2 seconds.

The simulation results are shown in Fig. 7 to Fig. 9.

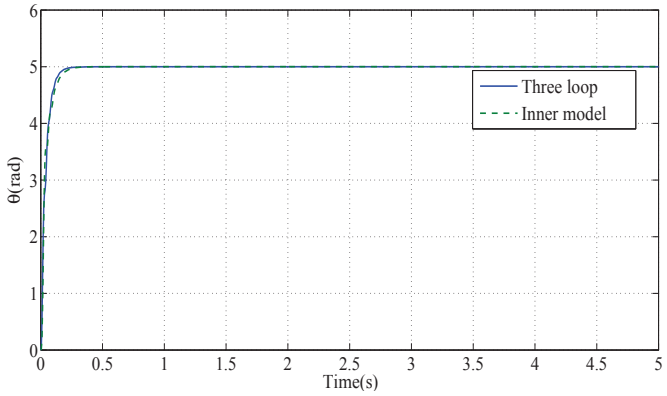

Fig. 7: The response of Three-loop and IMC control method without disturbance and parameter variation.

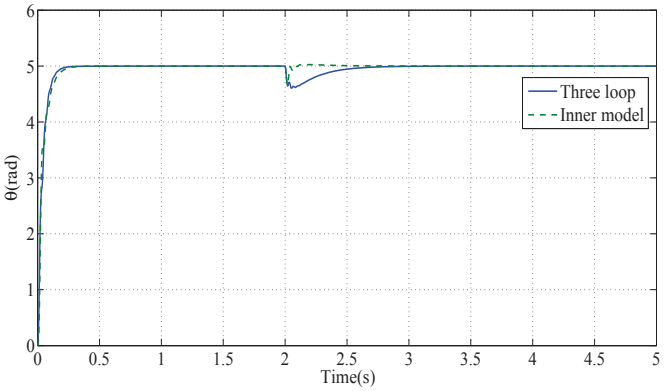

Fig. 8: The response of Three-loop and IMC control method with disturbance.

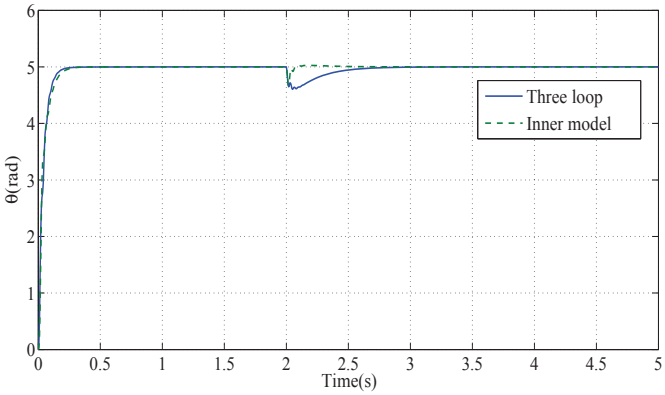

Fig. 9: The response of Three-loop and IMC control method with disturbance and parameter variation.

From Fig. 7 we can conclude that the two control methods have the similar dynamic performance in the ideal environment. But Fig. 8 and Fig. 9 show that the robustness performance of IMC method is better than the Three-loop control method in the environment with disturbance and parameter variation. And the IMC controller is designed with just two adjustable parameters, which is convenient. Parameters lists are shown in Table I and Table II.

TABLE I: Parameters of the PMSM

Parameter	Meaning	Value	Unit
L	rotator inductance	0.00027	H
R	rotator resistance	13	Ω
P_n	number of pairs	1	/
J	movement of initial	0.0062	Kg·m^2
K_e	torque constant	0.167	/
τ_V	inverter time constant	0.0001	s
K_n	inverter gain	4.43	/
K_s	proportionality coefficient	$5/\pi$	/

C. Force control design

Redundant branch could optimize the active stiffness and the driving forces. But because of the redundant branch, the control process of the 6PUS-UPU mechanism become more

TABLE II: Parameters of controller

Parameter	Meaning	Value	Unit
K_P	the proportional parameter of G_{APR}	15	/
K_V	the proportional parameter of G_{ASR}	1	/
T_V	the integral parameter of G_{ASR}	5	/
K_I	the proportional parameter of G_{ACR}	5.98	/
T_I	the integral parameter of G_{ACR}	0.0075	/
λ_1	filter parameter of IMC	0.008	/
λ_2	filter parameter of IMC	0.023	/

complex, the control model of the redundant branch is related not only to the kinestate complex, uncertain and nonlinear.

Because of its advantage of precise mathematical model, good robustness and simple design processes, fuzzy control is used in the systems with large-lag delay, nonlinearity, and the systems could not be obtained with precise mathematical model. But the basic fuzzy controller may lead to imperfect control results, such as steady state error [30]. Therefore, many methods are proposed by researchers to improve the fuzzy control. Fuzzy control combined with the PID (proportional-integral-derivative) control is a common method. In this paper, we employ the fuzzy-PID controller which combines the fuzzy logic and PID control techniques. Fig. 10 shows the diagram of the Fuzzy-PID control method [30].

where e is the error between the given input and the output, ec means the differential of e. The output of the basic fuzzy controller Δu, can be expressed as

$$\Delta u = K_u \cdot F\left[K_e \cdot e, K_{ec} \cdot ec\right] \tag{24}$$

where $F[\cdot]$ means some kind of mapping relationship between the input and output. Based on [31], Δu, is discrete, and can be expressed approximatively as

$$\Delta u(k) = K_1 e(k) + K_2 ec(k) \tag{25}$$

From (24) and (25), the output of the fuzzy-PID controller can be expressed as

$$\begin{aligned} u(k) =& K_I \frac{T}{1-z^{-1}} \Delta u(k) + K_P \Delta u(k) \\ =& \underbrace{K_I K_1 \frac{T}{1-z^{-1}} e(k)}_{Integration\ part} + \underbrace{(K_I K_2 + K_P K_1) e(k)}_{Proportion\ part} \\ &+ \underbrace{K_P K_2 ec(k)}_{Differentiation\ part} \end{aligned} \tag{26}$$

As it is shown in Fig. 10, the implementation of the Fuzzy-PID controller requires several parts, they are scaling factors, fuzzification, rule base, inference engine and defuzzification.

D. Fractional order Fuzzy-PID

In the traditional control theory, no matter the differential or the integral, it is integer order. Since 1980s, the research of the Fractional Order Calculus (FOC) has extended from the pure math field to the control theory [32]. And in the last few years, FOC has been combined with the fuzzy control theory [33]. In this paper, we combine the Fuzzy-PID control method with fractional order differential and integral operators, then propose a kind of Fractional Order Fuzzy-PID (FOFP) control method, and its diagram is shown in Fig. 11.

Where the α and β represent the power of the differential and integral. There are many definitions about fractional order calculus, but the Grunwald-Lernikov definition is mostly used in the control theory. It can be expressed as follows [32]:

$$\begin{aligned} {}_aD_t{}^{\alpha} f(t) &= \lim_{h\to 0} \frac{1}{h^{\alpha}} \sum_{j=0}^{[(t-a)/h]} (-1)^j \binom{\alpha}{j} f(t-jh) \\ &= \begin{cases} \dfrac{d^{\alpha}}{dt^{\alpha}} & \alpha > 0 \\ 1 & \alpha = 0 \\ \displaystyle\int_a^t (dt)^{\alpha} & \alpha < 0 \end{cases} \end{aligned} \tag{27}$$

where a is the initial condition, in general a = 0. α is the fractional order.

As we can see from (27), the implementation of fractional order differential or integral needs the exact expression of $f(t)$. But in the control field, the signal in the system cannot be expressed exactly in math. Filter is the mostly used method to implement fractional order differential or integral [34]. Among the many filters, the Oustaloup filter is preferred over others because of its outstanding approximation. Because the response of the differential or integral operator is a line in the full-frequency band, any kind of filter can approximate fractional order differential or integral operator in a certain band. We suppose that the frequency band is (w_b, w_h), the approximating transfer function provided by Oustaloup is as follows:

$$s^{\alpha} = K \prod_{k=-N}^{N} \frac{s + w_k{}'}{s + w_k} \tag{28}$$

where

$$\begin{cases} w_k{}' = w_b \left(\frac{w_h}{w_b}\right)^{\frac{k+N+\frac{1}{2}(1-\alpha)}{2N+1}} \\ w_k = w_b \left(\frac{w_h}{w_b}\right)^{\frac{k+N+\frac{1}{2}(1+\alpha)}{2N+1}} \\ K = w_h^{\alpha} \end{cases} \tag{29}$$

α is the order of the differential. N is the order of the filter, in general, N = 4. Now we suppose that the the order of the differential is 0.5, and the frequency band is (0.01,100), namely α = 0.5, w_b = 0.01 and w_h = 100. Its Bode diagram is shown in Fig. 12.

As we can see from Fig. 12, the approximation is unsatisfactory at the two endpoints in the range of (w_b, w_h). So in this paper, we take the improved Oustaloup filter to implement the fractional order differential operator. Its transfer function can be expressed as follows [35]:

$$s^{\alpha} \approx \left(\frac{dw_h}{b}\right)^{\alpha} \left(\frac{ds^2 + bw_h s}{d(1-\alpha)s^2 + bw_h s + d\alpha}\right) \prod_{k=-N}^{N} \frac{s + w_k{}'}{s + w_k} \tag{30}$$

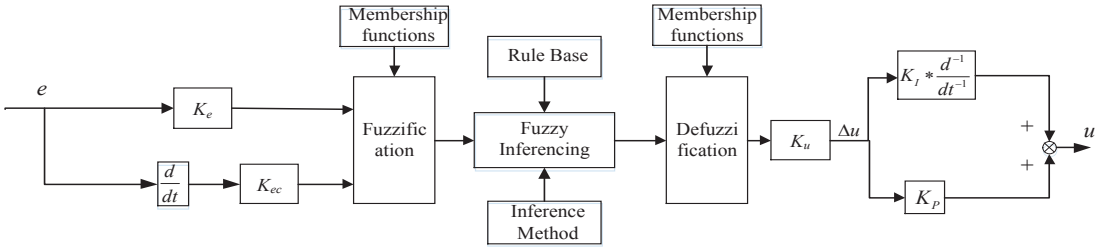

Fig. 10: The diagram of the fuzzy-PID control method.

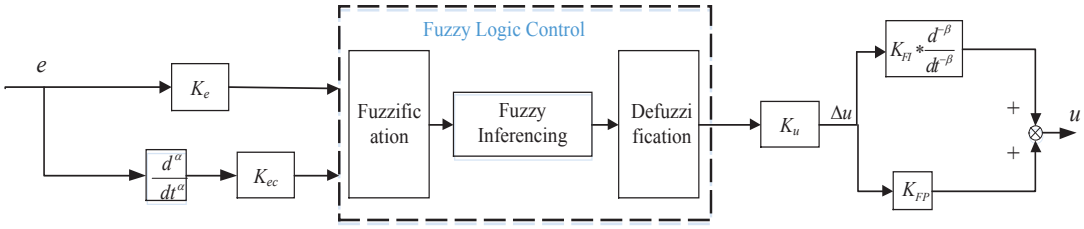

Fig. 11: The diagram of Fractional Order Fuzzy-PID (FOFP) control method.

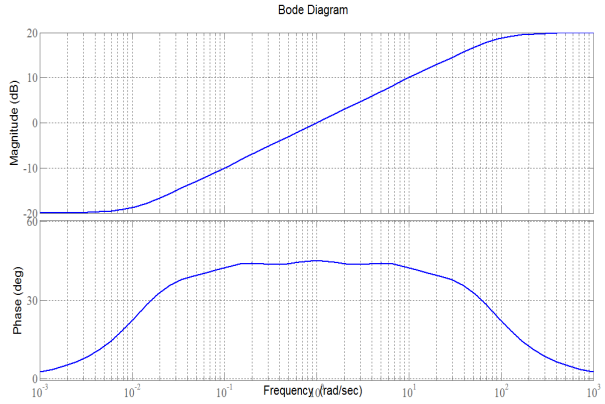

Fig. 12: The Bode diagram of the Oustaloup filter.

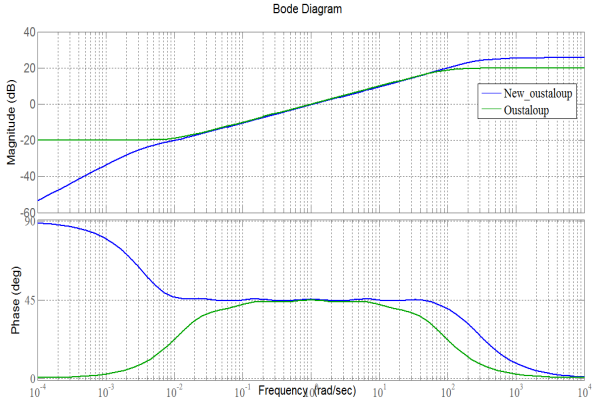

Fig. 13: The comparison Bode diagram of the Oustaloup filter and the improved Oustaloup filter.

where

$$w_k{}' = \left(\frac{dw_b}{b}\right)^{\frac{\alpha-2k}{2N+1}}, w_k = \left(\frac{bw_h}{d}\right)^{\frac{\alpha+2k}{2N+1}}$$

In general, $b = 10$, $d = 9$. Now we still suppose that the the order of the differential is 0.5, and the frequency band is (0.01,100), namely α = 0.5, w_b = 0.01 and w_h = 100. The Bode diagram of these two filter is shown in Fig. 13.

Obviously, the approximation of the improved Oustaloup filter is better than the Oustaloup filter, especially at the endpoints.

IV. Simulation Results and Discussion

In this section, the results obtained from trajectory tracking and noise suppression from control methods are discussed. The main parameters are shown in Table I to Table II. The desired trajectory of the platform is assumed. These numbers are the coordinates of the center of the movable platform. As

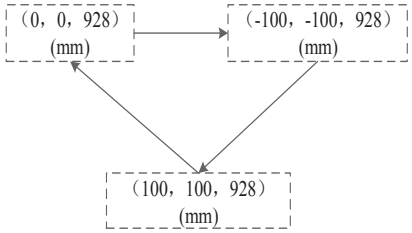

Fig. 14: The desired trajectory of the moveable platform.

for the redundant branch, the fourth order new Oustaloup's approximation is used with $N = 4$ and range of frequency $\omega \in [10^{-2}, 10^{2}]$ for the implementation of fractional order operator.

A. Three-loop + Fuzzy-PID

In this part, the first five branches use the Three-loop control method and the Fuzzy-PID control method is used

in the redundant branch. According to the application of the 6PUS-UPU, the shocks and overshoots of the position tracking are forbidden. So the first five branches are designed as damped and the damping ratio $\zeta_j \geq 1$, in this paper $\zeta_j = 1, j = 1, 2, ..., 5$. In order to obtain a short settling time, cut-off frequency (ω_j) is designed as $\omega_j = 10\pi$. To testify the performance of the Fuzzy-PID control method, the PI commonly used in the practical engineering is used in the redundant branch. The simulation results are shown in Fig. 15 to Fig. 22.

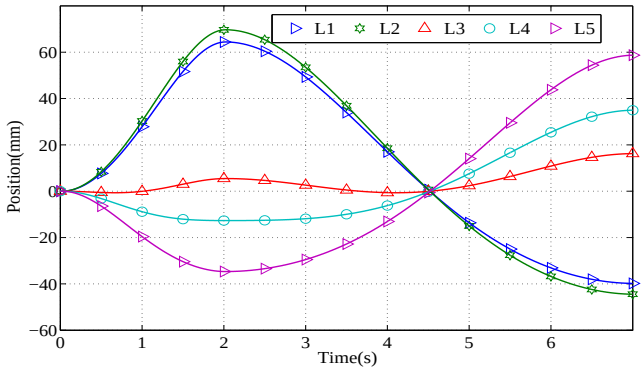

Fig. 15: The ideal trajectory for the first five branches.

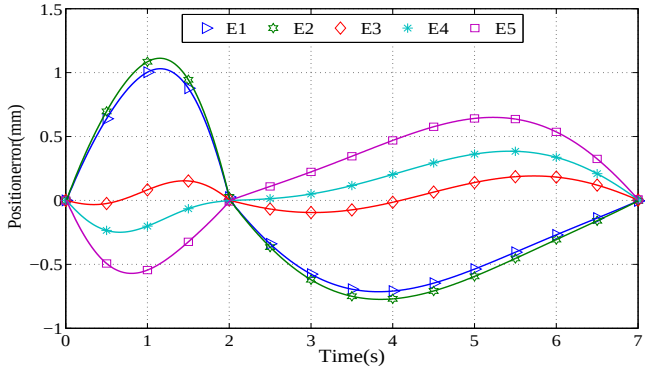

Fig. 16: The position errors of the first five branches under Three-loop + Fuzzy-PID control method without noise.

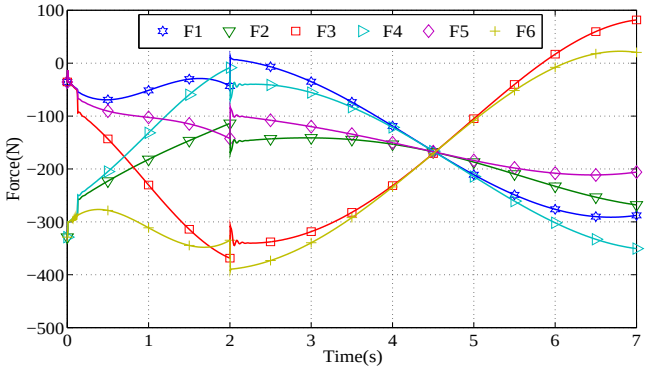

Fig. 17: The driving forces of six branches under Three-loop + Fuzzy-PID control method without noise.

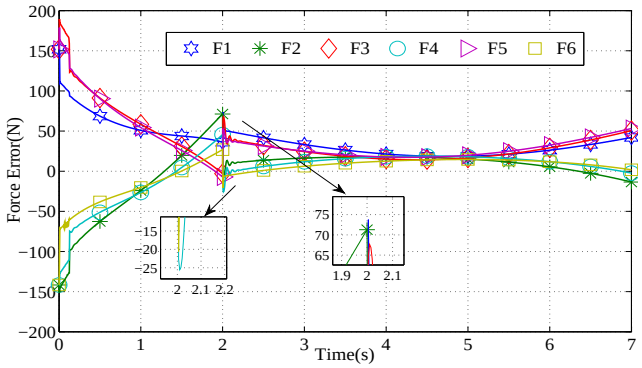

Fig. 18: The driving forces errors of six branches under Three-loop + Fuzzy-PID control method without noise.

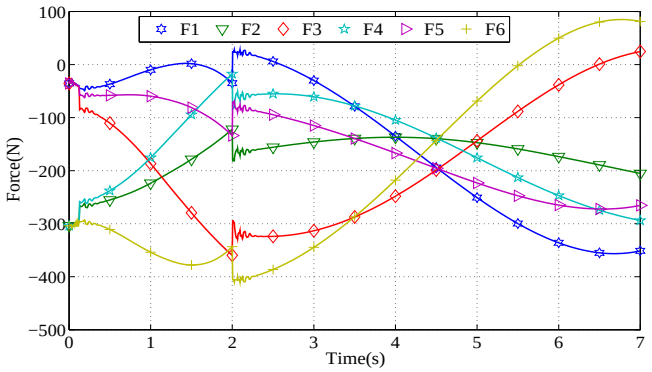

Fig. 19: The driving forces of six branches under Three-loop + PI control method without noise.

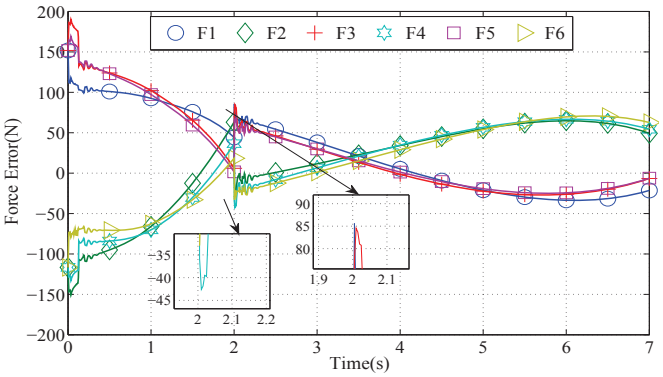

Fig. 20: The driving forces errors of six branches under Three-loop + PI control method without noise.

As we can see from Fig. 15 and Fig. 16, the position errors of the first five branches are between (-1, -1.5) mm. The more faster the branch moves, the bigger error it takes. Because the Three-loop control method takes the conventional controllers (P, PI, PI), it could not obtain satisfactory results under the complicated environment.

As we can see from Fig. 17 to Fig. 20, the force tracking performance of the Fuzzy-PID control method is obviously better than that of the PI control method. To further show that the Fuzzy-PID control method is superior to the PI control

method under interference, we add Gaussian noise into the redundant branch and test its robust property. Fig. 21 and Fig. 22 show the suppression performance results.

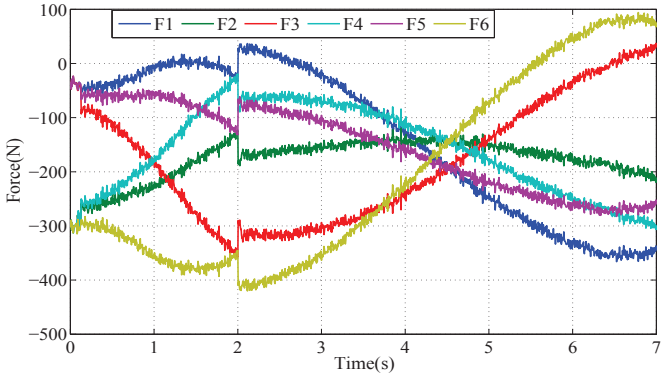

Fig. 21: The driving forces of six branches under Three-loop + PI control method with noise.

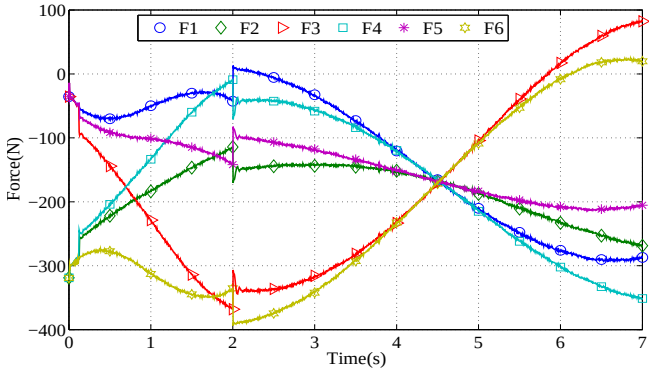

Fig. 22: The driving forces of six branches under Three-loop + Fuzzy-PID control method with noise.

It can be seen from Fig. 21 and Fig. 22 that the Fuzzy-PID control method could effectively eliminate the interference, meanwhile it gets better tracking performance. The PI control method is a kind of compromise scheme. When one of the parameters is adjusted to satisfy the anti-performance, the tracking performance could be degraded.

To compare the performance of the Fuzzy-PID control method and the PI control method, the force error curves are analyzed and the average amplitude errors are applied to establish the evaluative standard:

$$I_{imp} = \frac{|E_F - E_T|}{|E_T|} \tag{31}$$

where E_F is the average value of the 1-norm value of the force error of the fuzzy -PID control method, E_T is the average value of the 1-norm of the force error of the PI control method, I_{imp} describes the improvement. The results are listed in Table III.

As we can see from Table III, the control performance is obviously improved. Because we make the 6^{th} branch as the redundant actuation branch, the performance corresponding to the 2^{nd}, 4^{th}, 6^{th} branches get significantly improved and the improvement is above 50%. The performance corresponding to the 1^{st}, 3^{rd}, 5^{th} branches gets comparatively less improvement, but the improvement is still above 10%.

TABLE III: The improvement of the Fuzzy-PID control method than the PI control method

Force	$E_F\,(N)$	$E_T\,(N)$	$I_{imp}\,(\%)$
1	37.12	45.60	18.60
2	23.00	46.54	50.53
3	36.78	43.97	16.35
4	19.79	46.49	57.80
5	37.13	41.75	11.07
6	14.53	43.41	66.28

B. IMC + Fractional Fuzzy-PID

In this part, the first five branches adopt the IMC control method and the Fractional Fuzzy-PID control method is used in the redundant branch. The parameters of IMC control method are just λ_1 and λ_2, they are designed as 0.008 and 0.023. As for the redundant branch, the power of differential operator is designed as 0.75 namely $s^{0.75}$, and the power of integral operator is designed as -0.1 namely $s^{-0.1}$. The other parameters are listed in Table II. The simulation results are shown in Fig. 23 to Fig. 27.

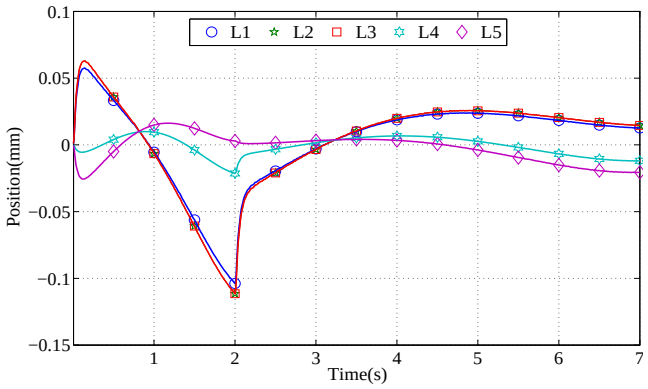

Fig. 23: The position errors of the first five branches under IMC + Fractional Fuzzy-PID control method without noise.

As we can see from Fig. 23, the IMC control method obviously outperforms the Three-loop control method. It narrows down the position errors to (-0.15, 0.1) mm, and Fig. 7 to Fig. 9 show that it has stronger robustness. Meanwhile, we just need to adjust two independent parameters, which is convenient. Comparing with PI and Fuzzy-PID control method, Fig. 26 shows that the Fractional Fuzzy-PID control method can further narrow down the driving forces errors. To testify its noise suppression performance, we add Gaussian noise into the redundant branch, and the result is shown in Fig. 27. It is similar to the Fuzzy-PID control method, the Fractional Fuzzy-PID control method which suppresses the noise interference

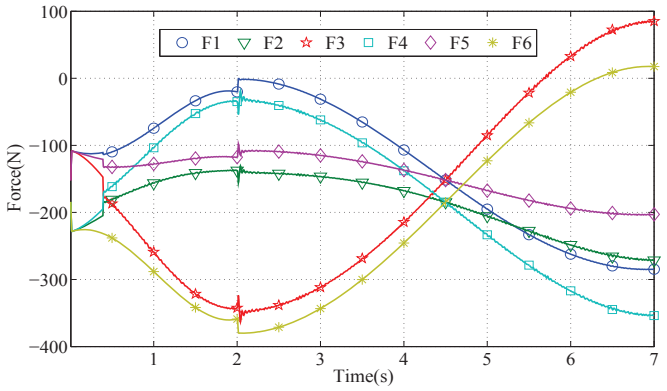

Fig. 24: The driving forces of six branches under IMC + Fractional Fuzzy-PID control method without noise.

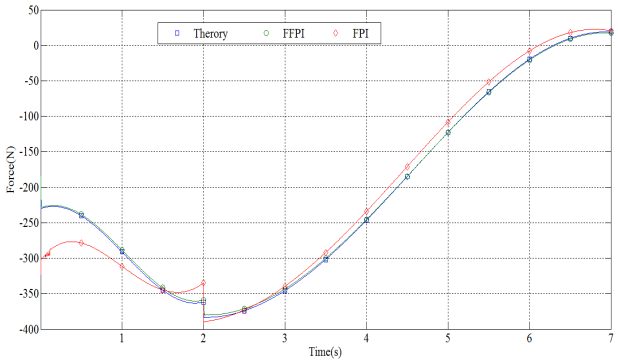

Fig. 25: Sixth branches in the three loop control, fractional order fuzzy PI control, fuzzy PI control diagram.

well. As Fig. 24 to Fig. 27 show the redundant branch using fractional fuzzy PI, tracking performance has improved significantly, the various branches of error is significantly reduced.

To quantificationally analyze the performance improvement of the Fractional Fuzzy-PID control method, the average value of the 1-norm values of the force error of the Fuzzy-PID and Fractional Fuzzy-PID control method are calculated, and the results are listed in the following Table IV.

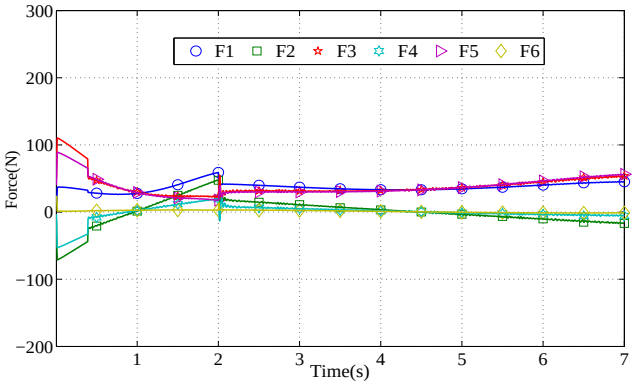

Fig. 26: The driving forces errors of six branches under IMC + Fractional Fuzzy-PID control method.

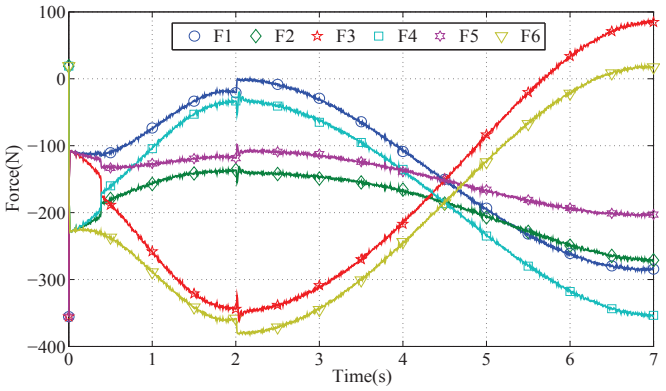

Fig. 27: The driving forces of six branches under IMC + Fractional Fuzzy-PID control method with noise.

TABLE IV: The improvement of the Fractional Fuzzy-PID control method than the Fuzzy-PID control method

Force	$E_F\,(N)$	$E_FF\,(N)$	$I_{imp}\,(\%)$
1	37.12	35.12	2.57
2	23.00	14.01	38.79
3	36.78	35.17	2.59
4	19.79	6.96	64.6
5	37.13	35.53	4.54
6	14.53	1.92	86.83

where E_F is the average value of the 1-norm value of the force error of Fuzzy-PID control method, E_FF is the average value of the 1-norm of the force error of Fractional Fuzzy-PID control method, I_{imp} describes the improvement. Comparing with the Fuzzy-PID control method, the improvement of 1^{st}, 3^{rd}, 5^{th} branch is smaller, but the driving forces of 2^{nd}, 4^{th}, 6^{th} branch are improved obviously.

V. Conclusions

In this paper, the IMC control method and Fractional Fuzzy-PID control method are designed in the trajectory tracking task of 6PUS-UPU parallel robot. The method of fractional operator based on the Fuzzy-PID control method improved the precision of the redundant branch of 6PUS-UPU parallel robot, and the IMC control method with two degrees of freedoms decreased the position error. The proposed control method in this paper was compared with other control methods, such as Three-loop control method, PI control method and Fuzzy-PID control method. In addition, the proposed method also has demonstrated good robustness under disturbance and noise. The results show that the IMC position controller and Fractional Fuzzy-PID redundant branch controller outperform other methods in trajectory tracking.

References

[1] X. Kong and C. Gosselin, *Type synthesis of parallel mechanisms*. Springer Publishing Company, 2007.

[2] S. Nokleby, R. Fisher, R. Podhorodeski, and F. Firmani, "Force capabilities of redundantly-actuated parallel manipulators," *Mechanism and Machine theory*, vol. 40, no. 5, pp. 578–599, 2005.

[3] W.-W. Shang, S. Cong, and Y. Ge, "Adaptive computed torque control for a parallel manipulator with redundant actuation," *Robotica*, vol. 30, no. 03, pp. 457–466, 2012.

[4] J. Wu, "Analysis, identification and control of a 4-DOF hybrid machine tool with actuation redundancy," Ph.D. dissertation, Beijing: Tsinghua Univesity, 2007.

[5] J. Qing, J. Li, and B. fang, "Drive optimization of tricept parallel mechanism with redundant actuation," *Journal of Mechanical Engineering*, no. 5, pp. 8–14, 2010.

[6] W. Liu and S. Chang, "Drive optimization of parallel robot under redundant tasks based on genetic algorithm," *Transactions of the Chinese Society for Agricultural Machinery*, vol. 43, no. 4, pp. 221–220, 2012.

[7] Q. Meng, T. Zhang, J. He, J. Song, and X. Chen, "Improved model-based control of a six-degree-of-freedom stewart platform driven by permanent magnet synchronous motors," *Industrial Robot: An International Journal*, vol. 39, no. 1, pp. 47–56, 2012.

[8] A. I. Savran, A. Beke, T. Kumbasar, and E. Yesil, "An imc based fuzzy self-tuning mechanism for fuzzy PID controllers," in *2015 International Symposium on Innovations in Intelligent SysTems and Applications (INISTA)*. IEEE, 2015, pp. 1–7.

[9] Y. Xu, Y. Zhao, Y. Kang, and R. Xiong, "Study on IMC-PID control for single-phase voltage-source ups inverters," in *2008 IEEE 3rd Conference on Industrial Electronics and Applications (ICIEA)*. IEEE, 2008, pp. 824–828.

[10] T. Shi, Z. Chen, and R. Tang, "Studying and realization of hydraulic servo system based on IMC," in *2009 International Conference on Measuring Technology and Mechatronics Automation (ICMTMA)*, vol. 3. IEEE, 2009, pp. 404–407.

[11] S. Bachir and C. Duvanaud, "Linearization of radio frequency amplifiers using nonlinear internal model control method," *AEU-International Journal of Electronics and Communications*, vol. 65, no. 6, pp. 495–501, 2011.

[12] X. Wei, K. Tsang, and W. Chan, "Non-linear PWM control of single-switch quadratic buck converters using internal model," *IET Power Electronics*, vol. 2, no. 5, pp. 475–483, 2009.

[13] X. Yang, C. Hua, J. Yan, and X. Guan, "An exact stability condition for bilateral teleoperation with delayed communication channel," *IEEE Transactions on Systems, Man, and Cybernetics, Part B: Cybernetics*, 2015.

[14] I. Podlubny, "Fractional-order systems and $PI^{\lambda}D^{\mu}$-controllers," *IEEE Transactions on Automatic Control*, vol. 44, no. 1, pp. 208–214, 1999.

[15] A. Rebai, K. Guesmi, D. Gozim, and B. Hemici, "Design of an optimized fractional order fuzzy-PID controller for a piezoelectric actuator," in *2014 15th International Conference on Sciences and Techniques of Automatic Control and Computer Engineering (STA)*. IEEE, 2014, pp. 456–461.

[16] P. Varshney and S. K. Gupta, "Implementation of fractional fuzzy PID controllers for control of fractional-order systems," in *2014 International Conference on Advances in Computing, Communications and Informatics (ICACCI)*. IEEE, 2014, pp. 1322–1328.

[17] S. Das, I. Pan, and S. Das, "Performance comparison of optimal fractional order hybrid fuzzy PID controllers for handling oscillatory fractional order processes with dead time," *ISA transactions*, vol. 52, no. 4, pp. 550–566, 2013.

[18] S. Das, I. Pan, S. Das, and A. Gupta, "A novel fractional order fuzzy-PID controller and its optimal time domain tuning based on integral performance indices," *Engineering Applications of Artificial Intelligence*, vol. 25, no. 2, pp. 430–442, 2012.

[19] D. I. Park, S. H. Lee, S. H. Kim, and Y. K. Kwak, "Torque distribution using a weighted pseudoinverse in a redundantly actuated mechanism," *Advanced Robotics*, vol. 17, no. 8, pp. 807–820, 2003.

[20] M.-J. Liu, C.-X. Li, and C.-N. Li, "Dynamics analysis of the gough-stewart platform manipulator," *IEEE Transactions on Robotics and Automation*, vol. 16, no. 1, pp. 94–98, 2000.

[21] A. Omran, A. Kassem, G. El-Bayoumi, and M. Bayoumi, "Mission-based optimal control of stewart manipulator," *Aircraft Engineering and Aerospace Technology*, vol. 81, no. 3, pp. 226–233, 2009.

[22] I. Davliakos and E. Papadopoulos, "Model-based control of a 6-DOF electrohydraulic stewart–gough platform," *Mechanism and Machine Theory*, vol. 43, no. 11, pp. 1385–1400, 2008.

[23] R.-M. Jan, C.-S. Tseng, and R.-J. Liu, "Robust PID control design for permanent magnet synchronous motor: a genetic approach," *Electric Power Systems Research*, vol. 78, no. 7, pp. 1161–1168, 2008.

[24] S. Li and H. Gu, "Fuzzy adaptive internal model control schemes for PMSM speed-regulation system," *IEEE Transactions on Industrial Informatics*, vol. 8, no. 4, pp. 767–779, 2012.

[25] J. Zhang, Z. Liu, and R. Pei, "Two-degree-of-freedom internal model control for AC servo system," *Transactions of China Electrotechnical Society*, vol. 4, p. 009, 2002.

[26] K. Watanabe and E. Muramatsu, "Adaptive internal model control of SISO systems," in *SICE 2003 Annual Conference*, vol. 3. IEEE, 2003, pp. 3084–3089.

[27] H. Liu and S. Li, "Speed control for PMSM servo system using predictive functional control and extended state observer," *IEEE Transactions on Industrial Electronics*, vol. 59, no. 2, pp. 1171–1183, 2012.

[28] Q. Jin, L. Qie, Q. Wang, Y. Tian, and Y. Wang, "PID controller design based on the time domain information of robust IMC controller using maximum sensitivity," *Chinese Journal of Chemical Engineering*, vol. 21, no. 5, pp. 529–536, 2013.

[29] H. Zhou, "Control technology research of 6PUS-UPU redundant driven parallel manipulator," Master's thesis, Yan Shan University, He Bei, China, May, 2014.

[30] H. X. Li and S. K. Tso, "Quantitative design and analysis of fuzzy proportional-integralderivative control a step towards autotuning," *International Journal of Systems Science*, vol. 31, no. 5, pp. 545–553, 2000.

[31] S. Mao and Y. He, "Design and performance analysis of fuzzy-PID controller," *Journal of Chinese Inertial Technology*, vol. 2, p. 13, 2006.

[32] R. Matusu, "Application of fractional order calculus to control theory," *International Journal of Mathematical Models and Methods in Applied Sciences*, vol. 5, no. 7, pp. 1162–1169, 2011.

[33] R. Sharma, K. Rana, and V. Kumar, "Performance analysis of fractional order fuzzy PID controllers applied to a robotic manipulator," *Expert Systems with Applications*, vol. 41, no. 9, pp. 4274–4289, 2014.

[34] A. Oustaloup, F. Levron, B. Mathieu, and F. Nanot, "Frequency-band complex noninteger differentiator: characterization and synthesis," *IEEE Transactions on Circuits and Systems I: Fundamental Theory and Applications*, vol. 47, no. 1, pp. 25–39, 2000.

[35] D. Xue, C. Zhao, and Y. Chen, "A modified approximation method of fractional order system," in *Proceedings of the 2006 IEEE International Conference on Mechatronics and Automation*. IEEE, 2006, pp. 1043–1048.

[36] Y. Yun and Y. Li, "Modeling and control analysis of a 3-PUPU dual compliant parallel manipulator for micro positioning and active vibration isolation," *Journal of Dynamic Systems, Measurement, and Control*, vol. 134, no. 2, pp. 021 001–9, 2012.

[37] D. Zhang and Z. Gao, "Forward kinematics, performance analysis, and multi-objective optimization of a bio-inspired parallel manipulator," *Robotics and Computer-Integrated Manufacturing*, vol. 28, no. 4, pp. 484–492, 2012.

APPENDIX

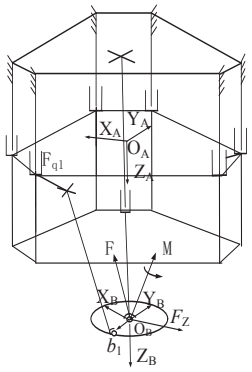

Fig. 28: The coordinate system of 6PUS-UPU redundant actuation parallel robot.

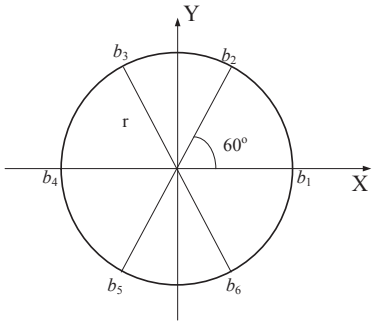

(a) Spherical hinge distribution diagram

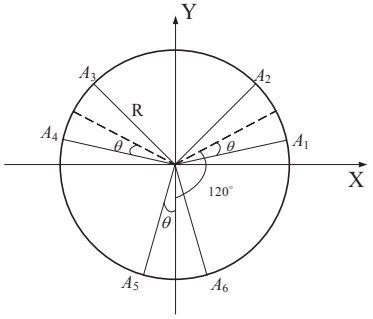

(b) Universal joint distribution diagram

Fig. 29: Distribution diagram of joint of 6PUS-UPU.

As we can see from Fig. 28, O_A and O_B are the origin of the fixed coordinate system and the movable coordinate, respectively. Fig. 29 shows the universal joint and spherical hinge distribution diagram. A_i represents the universal pair, b_i represents the sphere pair.

A. Velocity analysis

$\boldsymbol{q} = [x, y, z, u, v, w]^T$ is the vector of the movable platform generalized coordinates in fixed coordinate system. $[u, v, w]^T$ is the Euler angels. $\dot{\boldsymbol{q}}$ and $\ddot{\boldsymbol{q}}$ are the velocity and accelerate vectors of the movable platform, respectively. In the Cartesian coordinate system, the movable platform velocity vector is given as

$$(\boldsymbol{v}_d, \boldsymbol{w}_d) = (\dot{x}, \dot{y}, \dot{z}, {}^A w_{Bx}, {}^A w_{By}, {}^A w_{Bz}). \tag{32}$$

The transforming relationship between the two coordinate systems can be expressed as follows

$$(\boldsymbol{v}_d, \boldsymbol{w}_d)^T = \boldsymbol{J}_D \dot{\boldsymbol{q}} \tag{33}$$

where $\boldsymbol{J}_D = \begin{bmatrix} \boldsymbol{I}_{3\times3} & \boldsymbol{O}_{3\times3} \\ \boldsymbol{O}_{3\times3} & \boldsymbol{J}_d \end{bmatrix}$ and $\boldsymbol{J}_d = \begin{bmatrix} 1 & 0 & s\beta \\ 0 & c\alpha & -s\alpha \\ 0 & s\alpha & c\alpha c\beta \end{bmatrix}$. $\boldsymbol{v}_d$ and $\boldsymbol{w}_d$ are the angular velocities. From Fig. 28 we can get the following equation.

$$\begin{cases} \boldsymbol{L}_i = \boldsymbol{B}_i - \boldsymbol{A}_i \\ \boldsymbol{B}_i = \boldsymbol{P} + {}^A\boldsymbol{R}_B \boldsymbol{r}_{bi} \end{cases}, (i = 1, 2, \cdots 6) \tag{34}$$

where $\boldsymbol{L}_i$ is the vector of each link, $\boldsymbol{P}$ is $\boldsymbol{O}_B$ which is the center of the movable platform, ${}^A\boldsymbol{R}_B$ is the transmission matrix, $\boldsymbol{r}_{bi}$ is the location vector of b_i in the movable coordinate system, $\boldsymbol{A}_i$ and $\boldsymbol{B}_i$ are the coordinates of A_i and b_i in the fixed coordinate system, respectively.

The elastic deformation is not considered so that the length of the link is a constant. So we can get the following equation

$$\begin{aligned} &L^2 = (B_{ix} - A_{ix})^2 + (B_{iy} - A_{iy})^2 + (B_{iz} - A_{iz})^2, \\ &i = 1, 2, \cdots 6 \end{aligned} \tag{35}$$

We suppose that the velocity of each slider is $\dot{\boldsymbol{l}}_i = \dot{\boldsymbol{A}}_{iz} = \boldsymbol{J}_{Hi}\dot{\boldsymbol{q}}$, based on the feature of this mechanism. $\dot{\boldsymbol{l}}_i = \dot{\boldsymbol{A}}_{iz} = \boldsymbol{J}_{Hi}\dot{\boldsymbol{q}}$. The velocity of the slider can be expressed as in the following equation in the fixed coordinate system.

$$\boldsymbol{v}_{Hi} = \begin{bmatrix} \boldsymbol{O}_{1\times6} \\ \boldsymbol{O}_{1\times6} \\ \boldsymbol{J}_{Hi} \end{bmatrix} \dot{\boldsymbol{q}} \tag{36}$$

Taking derivative of (36), we can obtain $\boldsymbol{J}_{Hi}$.

The velocity of b_i in the fixed coordinate system can be expressed as

$$\boldsymbol{v}_{bi} = \boldsymbol{v}_{Hi} + \boldsymbol{w}_{Li} \times \boldsymbol{n}_i L \tag{37}$$

where $\boldsymbol{w}_{Li}$ is the angular velocity of the link, $\boldsymbol{n}_i = (\boldsymbol{B}_i - \boldsymbol{A}_i)/L$ is the unit vector of the link. Then we can get the angular velocity of the linkage as follows

$$\boldsymbol{w}_{Li} = \frac{\boldsymbol{n}_i \times (\boldsymbol{v}_d + \boldsymbol{w}_d \times \boldsymbol{r}_{Bi} - \boldsymbol{v}_{Hi})}{L} \tag{38}$$

where $\boldsymbol{r}_{Bi} = {}^A\boldsymbol{R}_B \boldsymbol{r}_{bi}$ is the location vector of b_i in the fixed coordinate system.

The linear velocity of the centroid of the linkage can be expressed as

$$\boldsymbol{v}_{Li} = \boldsymbol{v}_{Hi} + \boldsymbol{w}_{Li} \times \boldsymbol{n}_i \frac{L}{2}. \tag{39}$$

The joint between the movable platform and the middle constraint (UPU) branch is regarded as b_7, then the velocity of b_7 can be expressed as

$$\boldsymbol{v}_{b7} = \dot{l}_z \boldsymbol{s} + \boldsymbol{w}_{lz} \times \boldsymbol{L}_z \tag{40}$$

where $\boldsymbol{L}_z = \boldsymbol{B}_7 - \boldsymbol{A}_7$ is the vector of the middle constraint (UPU) branch, l_z is the length of the middle constraint (UPU) branch, $\boldsymbol{s} = \boldsymbol{L}_z/l_z$ is the unit vector of the middle constraint (UPU) branch. Then we can get the angular velocity $\boldsymbol{w}_{Lz}$ as follows

$$\boldsymbol{w}_{Lz} = \frac{\boldsymbol{s} \times (\boldsymbol{v}_d + \boldsymbol{w}_d \times \boldsymbol{r}_{B7})}{l_z} \tag{41}$$

where $\boldsymbol{r}_{B7} = {}^A\boldsymbol{R}_B \boldsymbol{r}_{b7}$ is the location vector of b_7 in the fixed coordinate system.

Therefore the centroid velocity of the upper and lower link of the middle constraint (UPU) branch can be expressed as

$$\begin{cases} \boldsymbol{v}_{zu} = \boldsymbol{w}_{Lz} \times \boldsymbol{s} l_u \\ \boldsymbol{v}_{zl} = \dot{\boldsymbol{l}}_z \boldsymbol{s} + \dot{\boldsymbol{w}}_{Lz} \times \boldsymbol{s} \left(l_u - l_l\right) \end{cases} \tag{42}$$

where l_u and l_l are the distance between the joint of the fixed platform and the centroid of the upper and the lower link, respectively, $\dot{\boldsymbol{l}}_z = \boldsymbol{v}_{b7}\boldsymbol{s}$ is the relative velocity between the upper link and lower link.

B. Acceleration analysis

The acceleration of the moveable platform can be expressed as

$$[\boldsymbol{a}_d \ \boldsymbol{\varepsilon}_d] = \dot{\boldsymbol{J}}_D \boldsymbol{q} + \boldsymbol{J}_D \dot{\boldsymbol{q}} \tag{43}$$

where $\boldsymbol{a}_d$ is the linear acceleration, $\boldsymbol{\varepsilon}_d$ is the angular acceleration.

The slider acceleration can be expressed as

$$\boldsymbol{a}_{Hi} = \begin{bmatrix} 0 & 0 & \ddot{\boldsymbol{l}}_i \end{bmatrix}^T \tag{44}$$

where $\ddot{\boldsymbol{l}}_i = \dot{\boldsymbol{J}}_{Hi}\dot{\boldsymbol{q}} + \boldsymbol{J}_{Hi}\ddot{\boldsymbol{q}}$.

The acceleration of b_i can be expressed as

$$\begin{cases} \boldsymbol{a}_{bi} = \boldsymbol{a}_d + \boldsymbol{\varepsilon}_d \times \boldsymbol{r}_{Bi} + \boldsymbol{w}_d \times (\boldsymbol{w}_d \times \boldsymbol{r}_{Bi}) \\ \boldsymbol{a}_{bi} = \boldsymbol{a}_{Hi} + \boldsymbol{\varepsilon}_{Li} \times \boldsymbol{n}_i L + \boldsymbol{w}_{Li} \times (\boldsymbol{w}_{Li} \times \boldsymbol{n}_i L) \end{cases} \tag{45}$$

where $\boldsymbol{\varepsilon_{Li}}$ is the angular acceleration of the link. Then we can get the link angular acceleration and centroid acceleration as follows

$$\begin{cases} \boldsymbol{\varepsilon}_{Li} = \boldsymbol{n}_i \times (\boldsymbol{a}_{bi} - \boldsymbol{a}_{Hi})/L \\ \boldsymbol{a}_{Li} = \boldsymbol{a}_{Hi} + \boldsymbol{\varepsilon}_{Li} \times \boldsymbol{n}_i L/2 + \boldsymbol{w}_{Li} \times \left(\boldsymbol{w}_{Li} \times \boldsymbol{n}_i L/2\right). \end{cases} \tag{46}$$

The acceleration of b_7 can be expressed as

$$\begin{cases} \boldsymbol{a}_{b7} = \boldsymbol{a}_d + \boldsymbol{\varepsilon}_d \times \boldsymbol{r}_{b7} + \boldsymbol{w}_d \left(\boldsymbol{w}_d \times \boldsymbol{r}_{b7}\right) \\ \boldsymbol{a}_{b7} = \boldsymbol{\varepsilon}_{Lz} \times \boldsymbol{L}_z + \boldsymbol{w}_{Lz} \times (\boldsymbol{w}_{Lz} \times \boldsymbol{L}_z) + \ddot{\boldsymbol{l}}_z \boldsymbol{s} + 2\boldsymbol{w}_{Lz} \times \dot{\boldsymbol{l}}_z \boldsymbol{s}. \end{cases} \tag{47}$$

The upper and lower link acceleration are expressed as

$$\begin{cases} \boldsymbol{a}_{zu} = \left[\boldsymbol{\varepsilon}_{Lz} \times \boldsymbol{s} + \boldsymbol{w}_{Lz} \times (\boldsymbol{w}_{Lz} \times \boldsymbol{s})\right] l_u \\ \boldsymbol{a}_{zd} = \left[\boldsymbol{\varepsilon}_{Lz} \times \boldsymbol{s} + \boldsymbol{w}_{Lz} \times (\boldsymbol{w}_{Lz} \times \boldsymbol{s})\right] (\boldsymbol{l}_z - \boldsymbol{l}_d) + \ddot{\boldsymbol{l}}_z \boldsymbol{s} + \\ \qquad\qquad 2\boldsymbol{w}_{Lz} \times \dot{\boldsymbol{l}}_z \boldsymbol{s}. \end{cases} \tag{48}$$

C. Partial velocity and angular velocity analysis

According to the definitions of partial velocity and angular velocity [36], we can obtain the partial velocity and angular velocity of each variable.

The partial linear and angular velocity of the movable platform are expressed as

$$\begin{cases} \boldsymbol{v}_d^* = [\boldsymbol{I}_3 \ \boldsymbol{O}_3] \\ \boldsymbol{w}_d^* = [\boldsymbol{O}_3 \ \boldsymbol{J}_d]. \end{cases} \tag{49}$$

The partial linear velocity of the slider is shown as

$$\boldsymbol{v}_{Hi}^* = [\boldsymbol{O}_{1\times 6}; \boldsymbol{O}_{1\times 6}; \boldsymbol{J}_{Hi}]. \tag{50}$$

The partial linear and angular velocity could be expressed as

$$\begin{cases} \boldsymbol{v}_{Li}^* = \boldsymbol{v}_{Hi}^* + \boldsymbol{w}_{Li}^* \times \boldsymbol{n}_i \cdot \frac{\boldsymbol{L}}{2} \\ \boldsymbol{w}_{Li}^* = \frac{\boldsymbol{n}_i \times (\boldsymbol{v}_d^* + \boldsymbol{w}_d^* \times \boldsymbol{r}_{bi} - \boldsymbol{v}_{Hi}^*)}{L}. \end{cases} \tag{51}$$

The partial linear and angular velocity of the middle constraint (UPU) branch are shown as

$$\begin{cases} \boldsymbol{w}_{Lz}^* = \frac{\boldsymbol{s} \times (\boldsymbol{v}_d^* + \boldsymbol{w}_d^* \times \boldsymbol{r}_{B7})}{l_z} \\ \boldsymbol{v}_{zu}^* = \boldsymbol{w}_{Lz}^* \times \boldsymbol{s} l_u \\ \boldsymbol{v}_{zd}^* = \boldsymbol{s}\dot{\boldsymbol{l}}_z^* + \boldsymbol{w}_{Lz}^* \times \boldsymbol{s} \left(l_z - l_d\right). \end{cases} \tag{52}$$

D. Constrain analysis

As we know from the the property of the machine, the movable platform is constrained by the middle branch which makes the mechanism more complicate. Based on the screw theory, we can get the constraints on spiral of the middle branch [37] as follows

$$\$^r = \begin{bmatrix} -\frac{\sin(\theta_2+\theta_4)\tan\theta_1}{d_3 \sin\theta_4} & \frac{\sin(\theta_2+\theta_4)}{d_3\sin\theta_4} & 0 \\ 1 & \tan\theta_1 & 0 \end{bmatrix} \tag{53}$$

where θ_1, θ_2, d_3 and θ_4 are the joint variables of the middle branch. If $\theta_2 + \theta_4 = 0$, the constraint of the middle branch is torque. If $\theta_2 + \theta_4 \neq 0$, the constraint is force. In this paper, we regard the constraint as $\boldsymbol{M}_c$ uniformly.